

Chapter 4

NMR Studies in Tetramethylammonium (TMA) Salts

NMR is a powerful technique for providing information about the reorientation and phase transitions. Temperature dependence of spin lattice relaxation time is useful in the study of structure and dynamics of the molecular groups present. Nature of molecular motions can be understood by interpreting the relaxation behaviour using suitable well-established models. Deviation of the observed results from the expected behaviour is also an useful information, which leads to the newer relaxation mechanisms. The observations of change of slope and discontinuities in T_1 along with the presence of hysteresis in T_1 have been recognized as the signature of different kinds of phase transitions [1-9].

Tetramethylammonium salts have captured the attention of both physicists as well as chemists for quite some time, because of their symmetry and interesting dynamics. Successive replacement of hydrogen by CH_3 groups in ammonium ion according to the formula $(\text{CH}_3)_x \text{NH}_{4-x}$ ($x = 1 \dots 4$), leads to a cation with a larger ionic radius, which may result in strong phase transitions due to changes in symmetry as well as the tolerance factor [10]. Substitution of the CH_3 leads to additional symmetry elements and hence increased reorientation motions [11]. Tetramethylammonium metal salts are known to exhibit phase transitions, hindered reorientational motion of the symmetry groups like CH_3 as well as whole cation $(\text{CH}_3)_4\text{N}$ and quantum rotational tunneling of the CH_3 groups. Moreover, Tetramethylammonium salts are of general interest in preparative chemistry. Their enhanced solubility in aprotic solvents in comparison to the corresponding alkali metal salts as well as their increased reactivity (which is due to a lower degree of solvation of their anions in solutions of non-polar solvents) make them powerful and versatile synthetic reagents [12].

This chapter contains the results of proton (and fluorine) NMR second moment as well as spin lattice relaxation time studies in Tetramethylammonium Selenate $[(\text{N}(\text{CH}_3)_4)_2\text{SeO}_4]$ and Tetramethylammonium Hexafluorophosphate $(\text{N}(\text{CH}_3)_4\text{PF}_6)$.

4.1 Tetramethylammonium Selenate $((\text{CH}_3)_4\text{N})_2\text{SeO}_4$

4.1.1 Introduction

A_2BX_4 (A = K, Rb, NH_4 , $\text{N}(\text{CH}_3)_4$ B = S, Zn, Cd, Ba, Cr, Hg, Se and X= Cl, Br, I, O etc) compounds are widely investigated and are still interesting to study, as they exhibit interesting incommensurate-commensurate phase transitions with temperature, ferroelectric properties and complex reorientational dynamics [13-17]. Recently, Horicuchi et al [18] have correlated their NMR results with single crystal x-ray results and Differential Scanning Calorimetry measurements to understand the nature of phase transitions in the similar compound $((\text{CH}_3)_3\text{CNH}_3)_2\text{ZnCl}_4$. The knowledge about the crystal chemistry of tetraalkylammonium salts is still limited [12], at least in tetraoxo complex salts $(\text{N}(\text{CH}_3)_4)_2\text{XO}_4$, which are of the pseudo A_2B -type. Tetramethylammonium Selenate (TMA-Selenate) is particularly interesting to study, not only for its interesting molecular reorientational dynamics but also due to its use in preparative chemistry [12].

4.1.2 Earlier studies

Sato et al [19] and Malchus et al [12] have prepared the compound TMA-Selenate. However, Malchus et al have reported that the compound prepared by Sato et al is not TMA-Selenate as they claim, but it is the hydrated one of TMA-Selenate. Two modifications (at 261 and 310 K) are characterized by X-ray diffraction methods and reported that, the compound crystallizes in a tetragonal lattice system with $a = 13.95$ and $c = 12.90 \text{ \AA}$ and also observed three heat anomalies at 127, 279 and 290 K through DTA. Sato et al have also reported ^1H NMR T_1 results in the temperature range 400 -200 K. Malchus et al [12] also have synthesized the same compound by adopting a different preparation method and carried out the temperature dependent single crystal XRD measurements and found a disagreement with that of Sato et al [19]. According to XRD analysis of Malchus et al, the compound crystallizes in cubic face centered crystal system ($\text{Fm}\bar{3}\text{m}$) with $a = 11.11 \text{ \AA}$ and the complex ions are packed in a Li_2O_2 -type arrangement. Further, in contrast to Sato et al, they have not reported any phase change in the temperature range 103 - 300 K. Coupled thermogravimetric and differential thermal analysis measurements [12] revealed the decomposition of the selenate in two exothermic

steps beginning at 503 ± 3 K and the third step is found to occur at 673 K resulting in a reddish-brown residue. IR and Raman studies by the same authors [12] have proved that, the $\text{N}(\text{CH}_3)_4^+$ tetrahedron is regular and in a fixed orientation, while the selenate ion, however, is orientationally disordered. To unravel the difference in XRD results, Malchus et al have carried out powder XRD study after exposing their compound to moisture and found that it compares well with the powdered XRD pattern reported by Sato et al [19]. Hence they have concluded that Sato et al might have studied the sample which was exposed to atmosphere and hence it might be the hydrate of tetramethylammonium selenate and not the $((\text{CH}_3)_4\text{N})_2\text{SeO}_4$ [12]. Thus, these studies lead to a controversy regarding the structure of this compound [12, 19]. Present study is an attempt to resolve this controversy. Figure 4.1 shows the unit cell of the refined model and the ORTEP plots of the complex ions and the characteristic parameters of TMA- Selenate are given in Table 4.1.

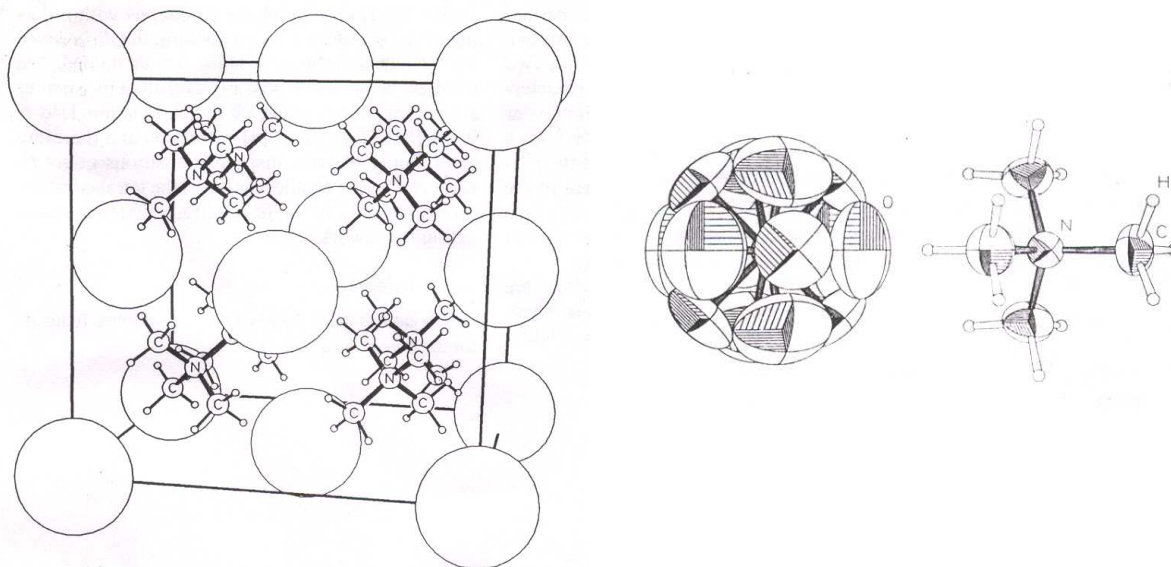


Figure 4.1 (a) Unit cell of TMA- Selenate (spheres represent the disordered Selenate ions) (b) Complex ions of TMA- Selenate (ORTEP plots with 50% probability level) [12]

Table 4.1 Characteristic parameters of TMA-Selenate [12]

Structure	Cubic
Space group	Fm $\bar{3}$ m
Cell dimension (a)	11.107 Å
Density	1.421 g cm ⁻³
Se-O (1)	1.63 Å
Se-O (2)	1.63 Å
N-C	1.49 Å
C-H	1.02 Å
C-N-C	109.5°
N-C-H	114°
Phase transitions	573 K 127 K, 279 K and 290 K [19]

Table 4.2. X-ray powder diffraction data of TMA-Selenate

d (Å) [Reported 12]	d (Å) [Present study]
6.416	6.418
3.928	3.925
3.350	3.348
2.779	2.782
2.485	2.490
2.138	2.140
1.965	1.964
1.878	1.880

4.1.3 Sample preparation and characterization

Different methods have been reported in the literature for the preparation of the TMA-Selenate [12, 19]. TMA-Selenate is synthesized by mixing tetramethylammonium hydroxide (Aldrich, 33,163-5) and Selenic acid (Aldrich, 30,843-9) in stoichiometric proportions [19]. Cylindrical crystals formed upon slow evaporation of the solvent, over a few months, are dried under vacuum before using them for further studies because of their hygroscopic nature. The Powder XRD measurements are carried out at room temperature using Panalytical diffractometer and the observed experimental d-spacings compare well with those reported by Malchus et al (Table 4.2) [12]. The compound is finely powdered and vacuum-sealed into glass ampoules of 5 mm diameter in helium atmosphere for NMR studies.

^1H NMR spin lattice relaxation time (T_1) measurements are carried out, as a function of temperature in the range 389 – 6.6 K, at 21.34 MHz using a home made pulsed NMR spectrometer described in Chapter 2 and inversion recovery pulse sequence is used for T_1 measurement over the entire temperature range.

4.1.4 Results and discussion

A plot of T_1 versus $1000/T$ is shown in Figure 4.2. Initially T_1 decreases with decrease in temperature from 389 K giving rise to a broad minimum of about 9 ms centered around 280 K. On further decrease in temperature, T_1 increases with a decrease in signal intensity and hence we could make measurements only up to 170 K and the signal vanishes completely around 150 K. On cooling the sample much below 150 K, the signal reappears at about 85 K and the signal intensity builds up enabling T_1 measurements from 72 K down to 6.6 K, which is the lowest temperature of measurement in the present study.

4.1.4.1 High temperature region (389 - 170 K)

Sato et al [19] have made T_1 measurements at 20 MHz in the temperature range 400 - 200 K. They have observed two minima: a shallow one (19 ms around 400 K) and another deep one (11 ms around 280 K), which are attributed to TMA and CH_3 group reorientations respectively. A theoretical fit of T_1 was extrapolated above 400 K to emphasize the shallow minimum. On the contrary, the present investigations reveal only

one broad minimum of about 9 ms around 280 K and on high temperature side of the minimum, T_1 increases monotonically up to 250 ms at 389 K. The high temperature (389 -170 K) T_1 data can be explained using Bloembergen-Purcell-Pound (BPP) model modified for TMA group by Albert et al [5].

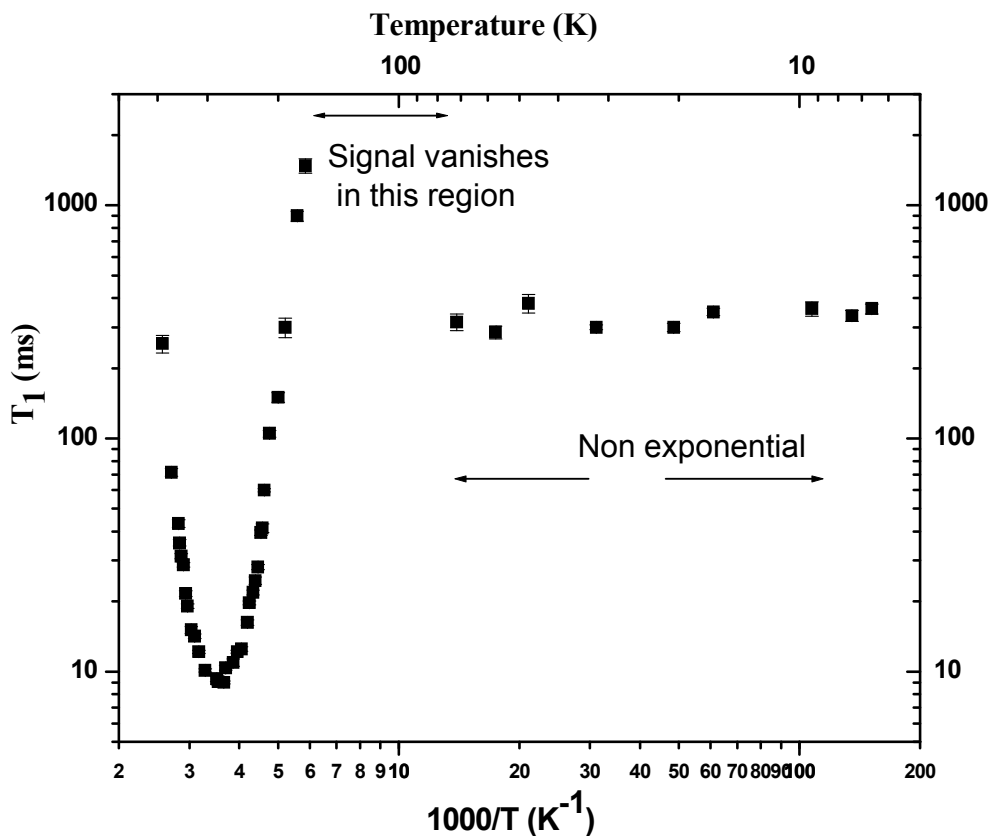


Figure 4.2 Variation of T_1 as a function of inverse temperature at 21.34 MHz for $(TMA)_2SeO_4$ over the entire temperature region (389 - 6.6 K).

Theory

Tetramethylammonium ion has tetrahedral symmetry (similar to the NH_4^+ ion). It has 3 two - fold and 4 three - fold symmetry axes. The T_1 behaviour in tetramethylammonium compounds can be explained using a modified BPP [20] approach, as given by Albert et al [5]. They have studied the 1H T_1 in several tetramethylammonium halides and the experimental results have been analyzed by considering the tetramethylammonium ion

and methyl group reorientations about their C_3 axes. In tetramethylammonium compounds, the two motions that mainly contribute to the relaxation are (a) random reorientation of the CH_3 groups with correlation time τ_c and (b) isotropic tumbling of the TMA ion (whole cation) with a correlation time τ_{c1} . They modulate the intra-methyl and inter-methyl dipole-dipole interactions and facilitate the spin-lattice relaxation.

The intra-methyl proton-proton interaction is modulated by the reorientations of the methyl groups about their C_3 axes. The relaxation rate due to the intra-methyl contribution is given by [5, 21]

$$T_{1(\text{intra})}^{-1} = \frac{9}{20} \frac{\gamma^4 \hbar^2}{r^6} \left(f(\omega, \tau_{c2}) + \frac{1}{3} f(\omega, \tau_{c1}) \right), \quad (4.1)$$

where,

$$f(\omega, \tau_c) = \frac{\tau_c}{1 + \omega_I^2 \tau_c^2} + \frac{4\tau_c}{1 + 4\omega_I^2 \tau_c^2} \quad (4.2)$$

and

$$\tau_{c2}^{-1} = \tau_c^{-1} + \tau_{c1}^{-1}. \quad (4.3)$$

In the above equations, $\gamma = 2.675 \times 10^4 \text{ G}^{-1} \text{ s}^{-1}$ is the nuclear gyromagnetic ratio of protons, ' τ ' represents a correlation time of the motion and is assumed to obey the Arrhenius equation given by

$$\tau = \tau_0 \exp(E_a / RT). \quad (4.4)$$

Here τ_0 and E_a are called pre-exponential factor and activation energy of the corresponding motion respectively.

The methyl group is considered as a three-spin system with 3 protons in each methyl group situated at the corners of the triangle and ' r ' is the inter proton distance within in the methyl group. Considering ' R ' as the distance between the centers of the proton triangles, then the relaxation rate due to the inter methyl proton-proton interaction, modulated by the tumbling of the TMA ion, is given by [5, 22]

$$T_{1(\text{inter})}^{-1} = \frac{27}{20} \frac{\gamma^4 \hbar^2}{R^6} f(\omega, \tau_{c1}). \quad (4.5)$$

The effective relaxation rate is the sum of the relaxation rates due to the intra-methyl and inter-methyl contributions and is given by [22]

$$T_1^{-1} = T_{1(\text{intra})}^{-1} + T_{1(\text{inter})}^{-1} \quad (4.6)$$

$$\text{i.e., } T_1^{-1} = A f(\omega, \tau_{c2}) + B f(\omega, \tau_{c1}) \quad (4.7)$$

where

$$A = \frac{9}{20} \frac{\gamma^4 \hbar^2}{r^6} \quad (4.8)$$

$$\text{and } B = \frac{3}{20} \frac{\gamma^4 \hbar^2}{r^6} + \frac{27}{10} \frac{\gamma^4 \hbar^2}{R^6} \quad (4.9)$$

Assuming that the TMA ion is an undistorted tetrahedron with C-H distance of 1.09 Å, C-N distance of 1.5 Å, the values of 'r' and 'R' calculated to be 1.78 Å and 3.04 Å respectively. Thus the values of A and B are found to be $A = 8.05 \times 10^9 \text{ sec}^{-2}$ and $B = 4.61 \times 10^9 \text{ sec}^{-2}$.

From Eqn. 4.7, one expects a minimum of 20.27 ms corresponding to the TMA tumbling motion, at $\omega\tau_{c1} = 0.616$ and another minimum of 11.74 ms corresponding to the CH₃ group reorientation at $\omega\tau_c = 0.616$ at the larmor frequency of 21.34 MHz. However, T₁ results in the present investigation reveals only one broad asymmetric minimum of 9 ms. The Albert et al model has been used for the analysis of T₁ results in the present compound and the fit is shown in Fig. 4.3. The best-fit parameters for CH₃ and TMA cation motions are given in Table 4.3.

The observed activation energies for both CH₃ and (CH₃)₄ ions obtained from the present study are respectively lesser than that of Sato et al [19] for the same compound (27 and 41 kJ/mol) as well as in ((CH₃)₄N)₂SO₄ (28 and 45 kJ/mol) and (CH₃)₄NX (X = Cl, Br and I) (23-28 and 37-54 kJ/mol) [8]. However, they are in good agreement with the values reported for the compound TMAClO₄ (21.2 and 32.9 kJ/mol) [23]. The CH₃ group activation energy is slightly greater than 15-17 kJ/mol and the (CH₃)₄ group activation energy compare well with the reported value of 30-37 kJ/mol, determined for the room temperature phase of [(CH₃)₄N]₂MX₄ (M=Pb and Pt ; X = Cl and Br) [24]. This shows an increased volume for reorientation of the groups as compared to pure salts. On comparing the activation energies of the CH₃ and (CH₃)₄N groups in ((CH₃)₄N)₂SeO₄

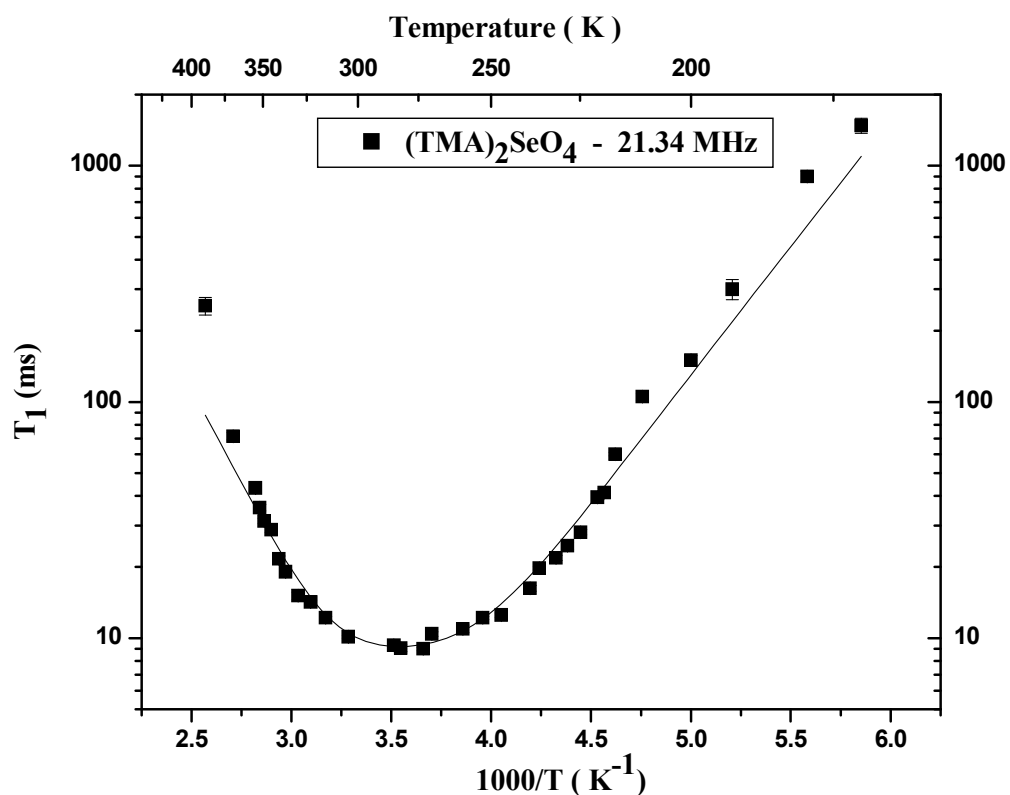


Figure 4.3 T_1 Versus $1000/T$ in the temperature region 389 – 170 K. Solid line represents the fit to Eqn. 4.7

Table 4.3. Motional parameters for TMA-Selenate in the temperature region (389 – 170 K). The values given in the parentheses represent the errors.

Symmetric group	Activation energy (kJ/mol)	Pre-exponential factor (10^{-13} s)
Methyl	20.4 (0.1)	5.3 (0.5)
TMA	33.5 (0.5)	0.09 (0.01)

with that of $((\text{CH}_3)_4\text{N})_2 \text{SO}_4$, it must be noticed that the activation energy of the methyl group is less in $((\text{CH}_3)_4\text{N})_2 \text{SeO}_4$ because of larger radius of selenium atom and its increased cell volume [19].

The observed asymmetric broad T_1 minimum of 9 ms at 21.34 MHz in our study is neither in agreement with that of expected minima of 11.74 ms for CH_3 group nor of 20.27 ms for $\text{N}(\text{CH}_3)_4$ group [5]. Similar broad minimum has been observed in many compounds like TMACl [5], TMAClO_4 [23], $\text{TMA}(\text{SnCl}_3)$ [25, 26] and $\text{TMA}(\text{HgBr}_3)$ [27]. The occurrence of this broad minimum could be due to the fact that, the reorientation rates of both methyl and TMA ions are of the same order. As discussed earlier, our powder XRD data do not agree with that of Sato et al, but agree quite well with those reported by Malchus et al, which confirms to the crystal structure as cubic. Further, it is also worth noting that the lower activation energies obtained from the present study, with respect to Sato et al, also suggest that, the symmetric groups are less hindered in the TMA-Selenate, as expected for a cubic system compared to tetragonal system. Therefore, both our NMR and powder XRD results support the argument of Malchus et al. Hence, we can conclude that, the compound used in the present study is in the cubic space group in agreement with that of Malchus et al [12] and not the hydrated TMA-Selenate as reported by Sato et al [19].

The increase of T_1 on the low temperature side of the T_1 minimum (from 170 K down to about 85 K) and a decrease of signal intensity beyond measurements and subsequent disappearance of the signal indicates that compound reaches rigid lattice limit at least in the NMR time scale.

4.1.4.2 Low temperature region (72 - 6.6 K)

On cooling the sample much below 150 K, the signal reappears at about 85 K and the signal intensity builds up enabling T_1 measurements from 72 K to 6.6 K. T_1 shows almost temperature independent behaviour in the temperature region 72 - 6.6 K. Further the magnetization recovery profile shows a deviation from both single exponential as well as bi-exponential fit. However, it fits well to a stretched exponential function at all

temperatures below 72 K down to 6.6 K with a varying stretched exponent. Figure 4.4 represents the typical magnetization recovery profile at 57.3 K and the insert within this figure shows the goodness of the fit to stretched exponential equation given by

$$M_z(\tau) = M_0 \left[1 - 2 e^{-\left(\frac{\tau}{T_1}\right)^\alpha} \right]. \quad (4.10)$$

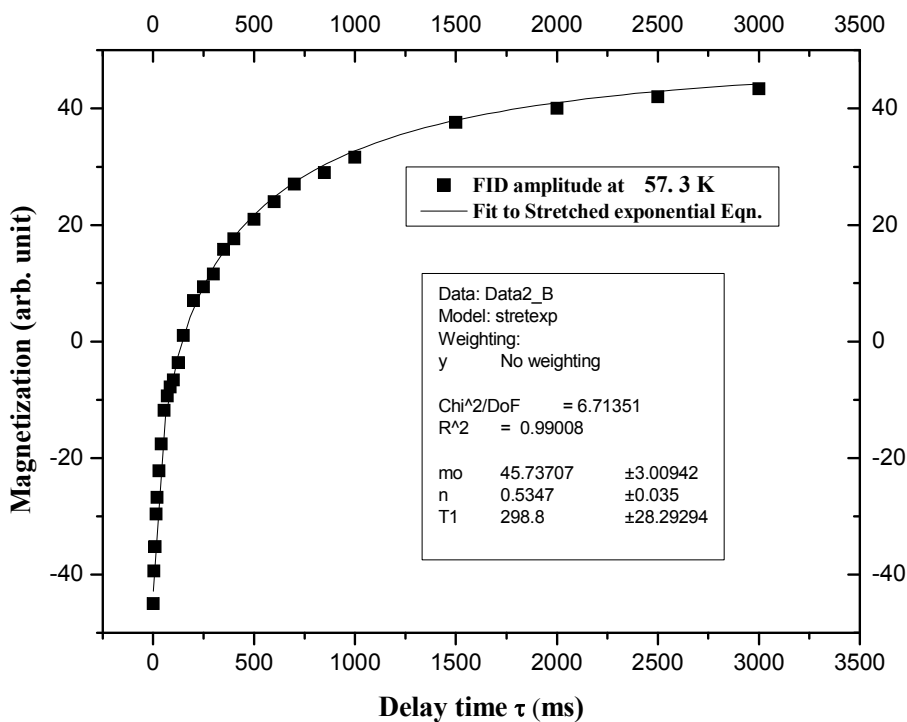


Figure 4.4 Magnetization recovery data versus τ plot for TMA-Selenate at 57.3 K. Solid line represents the fit to stretched exponential equation 4.10.

In this case, the repetition time of the inversion recovery pulse sequence is kept longer than 10 times the spin-lattice relaxation time so that the weight of the slowly relaxing components is also taken care. The value of exponent factor is about 0.5 when the signal reappears and it remains same within experimental errors till about 30 K. Below 30 K, the stretched exponent value increases monotonically and reaches unity as

the temperature approaches 6.6 K. All these features points to conclude the presence of quantum rotational tunneling of the methyl groups.

Effects of rotational tunneling of CH_3 and NH_4 groups on proton spin-lattice relaxation have been discussed by several authors [1, 2, 26, 28-38] to explain the non-exponential magnetization recovery and multiple T_1 minima at low temperatures.

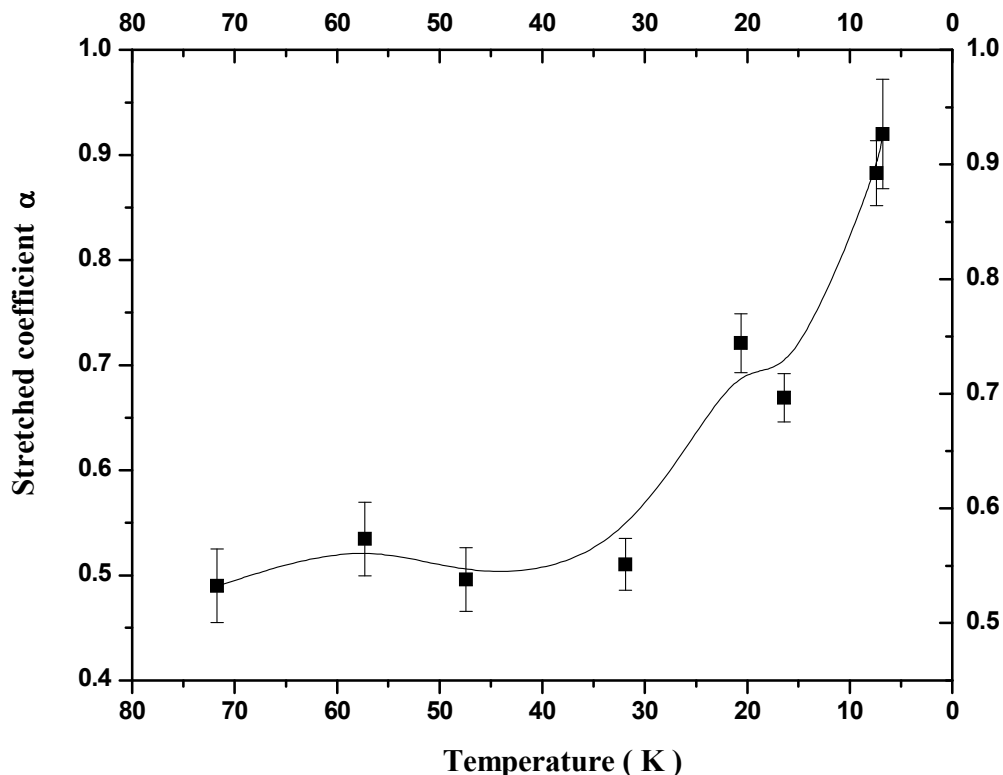


Figure 4.5 Variation of stretched exponent factor (α) with temperature. The line drawn is a guide to the eye.

Variation of the stretched exponent (Fig. 4.5) with temperature can be explained in the following way. In certain systems, the presence of inequivalent CH_3 groups may lead to different spin temperatures and each set of spins relaxing with its own relaxation time constant, and hence the bulk magnetization recovery follows a stretched exponential behaviour. This is true when inequivalent CH_3 groups are present and if the spin diffusion

becomes weaker in certain range of temperatures. However, when the temperature is lowered, the stretched exponent approaches unity, suggesting that the inequivalent methyl groups start attaining a common spin temperature. On further cooling the sample, the bulk magnetization recovery becomes single exponential.

In the present case, T_1 shows almost temperature independent behaviour and we have tried to fit our T_1 results using the model proposed by Koksals et al [39] who also have observed similar behaviour in certain metal acetates. According to the model proposed by them, T_1 shows temperature independent behaviour when only ground state of the tunnel splitting levels are occupied.

Theory

Koksals et al [39] have studied a number of metal acetates by ^1H NMR T_1 measurements and explained their experimental results by considering temperature dependence of tunnel splitting. At low temperatures, it is assumed that only the torsional ground state ($n = 0$) of the methyl group is occupied. The relaxation occurs when spin-flips are connected with the tunnel splittings. When the tunneling frequency is larger than the Larmor frequency, one can write the expression for the relaxation rate by considering only the intra-methyl interaction and temperature dependence of the tunnel frequency, as

$$\frac{1}{T_{AE}} = C_{AE} \sum_{m=-2}^2 \frac{m^2 \tau_{c0}^T}{1 + \langle \omega_T^0 \rangle^2 (\tau_{c0}^T)^2} \quad (4.11)$$

where ω_T^0 is the tunnel frequency in the ground state

$$\text{and } C_{AE} = \frac{9}{20} \frac{\gamma^4 \hbar^2}{r^6} d_0^2 \quad (4.12)$$

In the Eqn. 4.12, ' r ' is the inter proton distance in the methyl group and d_0 is the matrix element of the space part of the dipolar operator between the ground state wave functions of the harmonic oscillator [39, 40].

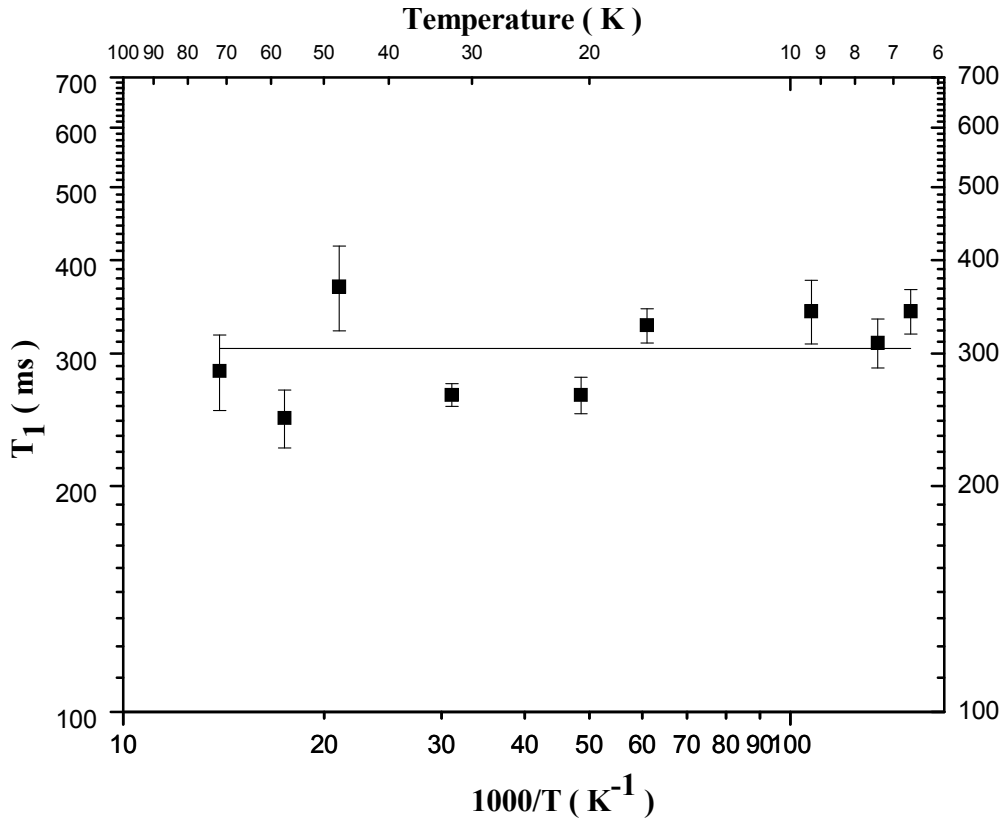


Figure 4.6 Low temperature (72 - 6.6 K) data. Solid line represents the fit to Eqn. 4.11.

Table 4.4 Motional parameters evaluated (72 - 6.6 K) using Koksai model [39].

Parameters	Estimated values
τ_{c0}^T	$5.26 \times 10^{-11} \text{ s}$
C_{AE}	$6.25 \times 10^9 \text{ s}^{-2}$
ω_T^0	$5.70 \times 10^9 \text{ s}^{-1}$

The T_1 data between 72 and 6.6 K is fit to the model used by Koksal et al and is shown in Fig. 4.6. The best-fit motional parameters obtained from the fit are given in Table 4.4, which are comparable with those reported earlier [26, 39]. Though the magnetization follows stretched exponential in this temperature region, the observed correlation time can be considered as the effective correlation time of the all spin systems.

4.1.5 Conclusions

A broad T_1 minimum observed in TMA – Selenate around 280 K is attributed to the simultaneous motions of CH_3 and $(\text{CH}_3)_4\text{N}$ groups. Lower activation energy obtained from the T_1 analysis as well as powder XRD measurements confirm that, the present compound crystallizes in cubic form and not as tetragonal. Magnetization recovery is found to be stretched exponential below 72 K with varying stretched exponent. Low temperature T_1 results show the quantum rotational tunneling of methyl groups and the observed T_1 is the resultant of the relaxation of all spin systems.

4.2 Tetramethylammonium Hexafluorophosphate $(\text{CH}_3)_4\text{NPF}_6$

4.2.1 Introduction

ABX_6 (A = K, Na, Rb, Cs, $\text{C}_5\text{H}_{10}\text{NH}_2$, $\text{C}_4\text{H}_8\text{NH}_2$, $\text{C}(\text{NH}_2)_3$, NH_4 , $\text{N}(\text{CH}_3)_4$, B = P and X = F) compounds have been investigated using different techniques as they exhibit phase transitions with temperatures, and complex reorientational dynamics [41 - 47]. The line shape and spin lattice relaxation studies of the fluorine NMR have been extensively carried out as a function of temperature in the polycrystalline sodium, potassium, rubidium and cesium hexafluorophosphates [41]. From these studies, it is concluded that the fluorine line shape is sensitive to the physical state and in the case of RbPF_6 , the thermal history of the sample and this behaviour is also observed in heat capacity measurements [48]. Motional narrowing of the dipolar broadening by PF_6^- reorientations

are found in all the samples studied and the temperature of its occurrence is found to increase monotonically from a temperature less than about 50 K for the cesium compound to about 155 K for the sodium. These effects are attributed to crystal defects, which lower the hindrance to reorientation of the PF_6^- ions and decrease the size of domains in which there is a cooperative 'freezing out' of the reorientations. Thus the samples exhibits two-phase behaviour, a phase without imperfections (or with fewer) in which the PF_6^- ions reorient more slowly than in a phase with a high (or higher) concentration of defects. This study along with the earlier very extensive NMR investigations of the ammonium and tetramethylammonium complexes in general and ammonium hexafluorophosphate in particular have suggested that it would be instructive to investigate tetramethylammonium hexafluorophosphate (TMA-Phosphate), in which the reorientations of both cation and anion groups are present. It is observed that, T_1 is often more sensitive to phase changes and cross relaxation than to line shape or second moment and its temperature dependence provides much more reliable values of the activation energies for the processes governing the relaxation.

In the present study, the proton and fluorine spin lattice relaxation time (T_1) and proton second moment measurements are undertaken in an analogues compound, TMA-Phosphate for the following reasons: (1) The three possible reorienting groups CH_3 , $\text{N}(\text{CH}_3)_4$ and PF_6^- are very well suited for NMR studies. (2) The importance of proton-fluorine dipolar interactions can be investigated. (3) The anions BF_6^- ($\text{B} = \text{P}, \text{Sb}$ and As) are known to form very weak hydrogen bonds [49] (4) The coexistence of two phases.

Further TMA-Phosphate is a promising candidate for technological applications Viz., in high energy density battery applications, as electrolyte for the preparation of the films, as electrolyte for preparation of films, as antifungal agent to make semiconductor films, as corrosive resistant material and in making opaque inkjet ink compositions [49A].

In the present study, commercially available TMA-Phosphate from Aldrich Chemicals [558-32-7] is used directly without further purification. The compound is

finely powdered and vacuum-sealed into glass ampoules of 5 mm diameter in helium atmosphere and then used for NMR measurements.

4.2.2 Earlier studies

Wang et al have reported the room temperature crystal structure of TMA-Phosphate [50]. The crystal structure of TMA-Phosphate indicates that even though the N- atom formally has a distorted tetrahedral symmetry ($\bar{4}2m - D_{2d}$), the cation can nevertheless be considered to be tetrahedral within experimental accuracy and the P atom has square-pyramidal symmetry (4mm). The infrared and Raman studies [47] have not revealed any phase transitions with temperature and the existence of ordered PF₆ groups. The characteristic parameters of TMA- Phosphate are given in Table 4.5. ³¹P NMR, DSC and X-ray powder diffraction measurements as a function of temperature have been carried out by Reynhardt et al [51]. DSC measurements from 120 to 800 K revealed three endothermic transitions, viz. at 770, 789 and 795 K. On lowering the temperature below 210 K, the X- ray diffractogram has shown additional peaks and the peak intensities increase with decreasing temperature and remain constant below 150 K. The additional peaks appearing below 210 K represent new diffraction plane, which is indexed by hexagonal unit cell. ³¹P NMR T₁ studies as a function of temperature at 81 MHz, revealed a single minimum of about 100 ms around 150 K. This observation is explained in terms of Miller and Gutowsky's two-phase model [41], through which they concluded that TMA- Phosphate contains two phases one with imperfections and another one without imperfections. ³¹P NMR T₁ studies yielded an activation energy of 15 ± 2 kJ/mol, $\tau_{co} = (6 \pm 2) \times 10^{-15}$ s for isotropic reorientation of all PF₆ ions.

4.2.3 Results and discussion

¹H NMR second moment (M₂) measurements are carried out, as a function of temperature in the temperature range 300 – 77 K, at 7 MHz using a home made wide-line NMR spectrometer described in Chapter 2 [52]. Second moment is calculated from the derivative of the absorption signal recorded using lock-in detection as described in Chapter 1.

Table 4.5. Characteristic parameters of TMA-Phosphate [50]

Structure	Tetragonal
Space group	P4/ nmm
Cell dimensions	a = 8.436 Å and c = 6.089 Å
Density	1.68 mg m ⁻³
PF ₆	4 mm
P-F (axial 1)	1.585 Å
P-F (axial 1)	1.591 Å
P-F (equatorial)	1.568 Å
F-P-F	90° or 180°
(CH ₃) ₄	$\bar{4}3m$
N-C	1.486 Å
C-H	1.06 Å
C-N-C	109.5°
N-C-H	107°
N-C-H	112°

¹H NMR spin lattice relaxation time (T₁) measurements are carried out, as a function of temperature, at three larmor frequencies 21.34 MHz, 16.1 MHz and 11.4 MHz, in the temperature range from 350 K down to liquid helium temperatures using a home made pulsed NMR spectrometer described in Chapter 2. Inversion recovery pulse sequence is used for the measurement of T₁ through out the temperature region studied.

^{19}F NMR spin lattice relaxation time (T_1) measurements are carried out, as a function of temperature, at two larmor frequencies 21.34 MHz and 16.1 MHz, in the temperature range from 320 K down to liquid helium temperatures. Inversion recovery pulse sequence is used for the measurement of T_1 except at higher temperatures where T_1 is higher than 1 s, saturation burst sequence is used. For both the nuclei studied (^1H and ^{19}F), the magnetization recovery is found to be single exponential within the experimental error throughout the temperature region studied.

4.2.3.1 Second moment

The second moment determined as a function of temperature in the range 300 -77 K is shown in Fig. 4.7. The second moment value remains almost constant of about $3 (\pm 0.2) \text{ G}^2$ in the temperature range 300 -180 K within the experimental error. Below 180 K, the signal starts broadening and second moment increases monotonically with the decrease of intensity. The lowest temperature at which the signal can be detected in this compound is 155 K with a second moment of $18 (\pm 1) \text{ G}^2$. Below this temperature, the signal is completely buried in noise and hence no second moment measurements are possible. Attempt to measure second moment at 77 K, by directly immersing the sample tube in liquid nitrogen dewar has also failed due to poor signal to noise ratio.

The theoretical dipolar second moment for a rigid array of nuclei in the crystal lattice can be calculated using the expression of Van Vleck [53]. There are many second moment simulation studies reported in the literature including those for Tetramethylammonium ion in different complexes [54-60]. The rigid lattice second moment can be calculated for a rigid $(\text{CH}_3)_4\text{N}$ ion using the formula [60]

$$M_2 = \frac{9}{10} \frac{\gamma^2 \hbar^2}{r^6} + \frac{81}{20} \frac{\gamma^2 \hbar^2}{R^6} + M_{HT} , \quad (4.13)$$

where $\gamma = 2.675 \times 10^4 \text{ G}^{-1} \text{ s}^{-1}$ is the nuclear gyromagnetic ratio of protons and M_2 is measured in G^2 . Following Albert et al [5], we have used $r = 1.78 \text{ \AA}$ as the distance between the protons belonging to the same CH_3 group and $R = 3.04 \text{ \AA}$ as the average distance between the protons belong to different groups, for the second moment

calculations. The high temperature residual second moment M_{HT} is considered to be 1 G^2 [62] and the estimated rigid lattice M_2 value is found to be 28 G^2 [59]. In the present

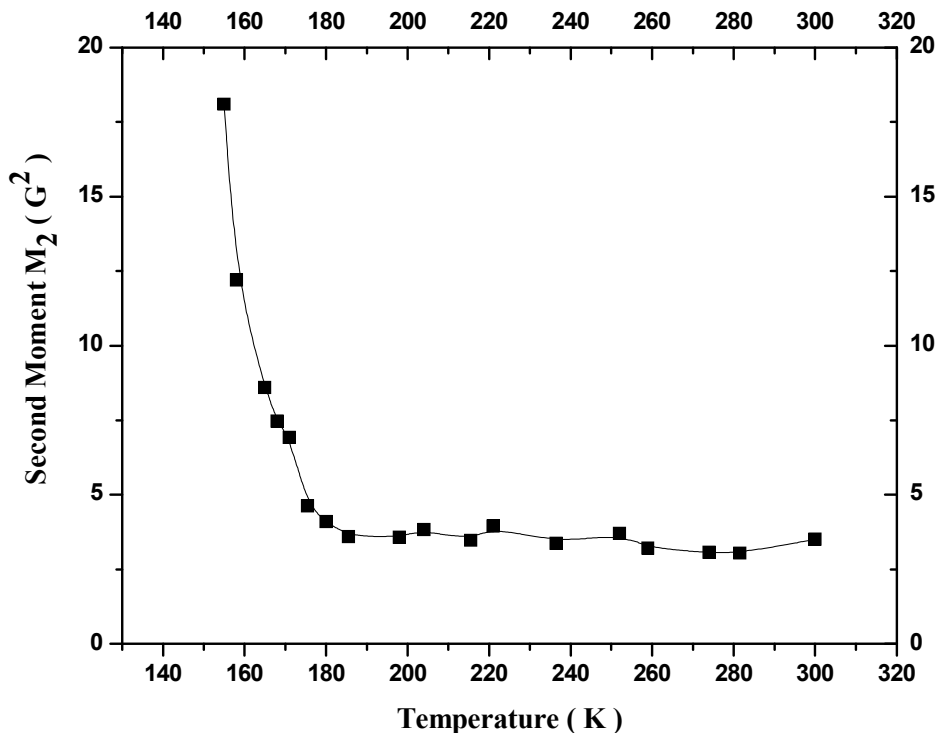


Fig. 4.7 ^1H NMR Second moment data of TMA-Phosphate at 7 MHz in the temperature region 300 -155 K; the line is guide to the eye.

investigations, the observed M_2 is only 18 G^2 at 155 K. However, second moment plot shows the tendency to increase further to rigid lattice limit at lower temperatures. Hence, the tendency of the second moment to reach its rigid lattice limit as well as the disappearance of the signal at 77 K suggest that, molecular motions responsible for motional narrowing of the signal start freezing at temperature below 180 K. We can estimate the activation energy from the formula $E_a = 155 T_C \text{ J/mol}$ [58], where T_C is the temperature at which the NMR spectrum narrows. The activation in the present investigation yields (for $T_C = 155 \text{ K}$) 24 kJ/mol suggesting the activation energy should be lower than this value. The observed plateau second moment of about 3 G^2 in the high

temperature region suggests that both TMA and methyl groups reorientations are active down to 180 K and below which, motions of both the groups start freezing. The present investigations show no resolved plateau in second moment, (two plateau regions are expected for TMA compounds) indicating that the two motions do not have widely differing correlation frequencies [60]. Since the line narrowing observed in this complex seems to occur in a single step, it can be concluded that the individual C_3 reorientation of four CH_3 groups in the cation and the overall reorientation of the cation as a whole occur simultaneously at a very narrow interval of temperature. Similar behaviour has been observed in $(CH_3)_4NCdCl_3$ [59], $(CH_3)_4NCl$ [60], and $((CH_3)_4N)_2MX_6$ ($M = Pt, Te$ and $Sn, X = Cl$ and Br) compounds [9, 63]. These results are consistent with our T_1 measurements discussed in the next section.

4.2.3.2 Spin lattice relaxation time

Figure 4.8 shows the variation of 1H and ^{19}F NMR spin lattice relaxation times (T_1) with inverse temperature ($1000/T$) over the entire temperature range studied. The ^{31}P T_1 data at 81 MHz in the same compound, reported by Reynhardt et al [51] is also included for comparison. The T_1 data are analyzed in two parts (a) 1H NMR spin lattice relaxation time studies as shown separately in Fig. 4.9 and (b) ^{19}F NMR spin lattice relaxation time studies as shown separately in Fig. 4.10.

(a) 1H NMR T_1 analysis

Figure 4.8 shows only the 1H NMR spin lattice relaxation time data at three larmor frequencies (11.4, 16.1 and 21.34 MHz). Initially T_1 decreases with decrease in temperature from 350 K giving rise to a single asymmetric minimum instead of two expected minima, corresponding to each symmetric groups (TMA and CH_3) present in the compound, as in most of the Tetramethylammonium compounds. T_1 minima of about 4.20, 5.42 and 7.35 ms observed respectively at 11.4, 16.1 and 21.34 MHz, around 190 K, suggest that this single minimum is unlikely to be solely due to the single group reorientation, but due to the resultant of both CH_3 and TMA group reorientations. On further decrease in temperature, T_1 increases with a decrease in signal intensity, at all

frequencies studied and hence we could make measurements only up to 150 K. The signal to noise ratio decreases drastically and signal vanishes completely below 150 K. The signal did not reappear, as in the case of TMA - Selenate, below 150 K and down to liquid helium temperatures.

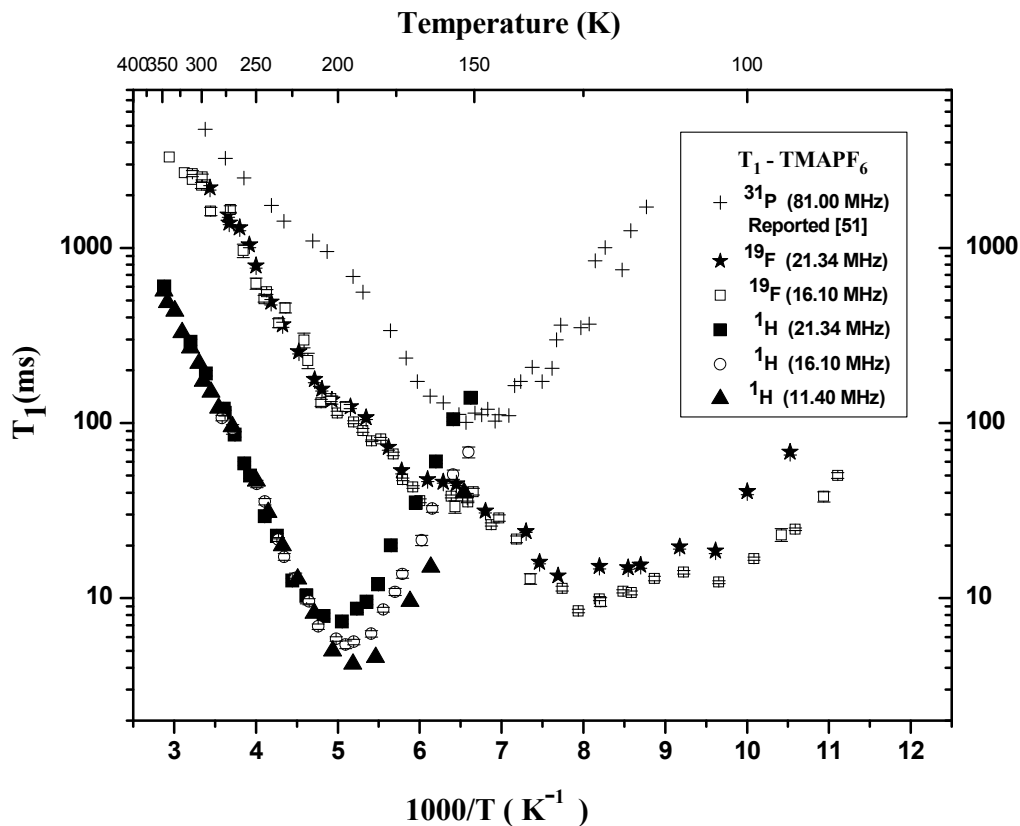


Figure 4.8 ^1H (11.4, 16.1 and 21.34 MHz), ^{19}F (16.1 and 21.34 MHz) and ^{31}P (Reynhardt et al [51] at 81 MHz) NMR T_1 versus $1000/T$ in TMA-Phosphate in the entire temperature range studied.

The ^1H T_1 behaviour can be explained using Albert et al [5] model as explained in the section 4.1.4.1. Here also, assuming that the TMA ion is an undistorted tetrahedron, with C-H distance of 1.09 Å and C-N distance of 1.5 Å, the values of r and R are calculated to be 1.78 Å and 3.04 Å respectively. The values of A and B are found to be

$A = 8.05 \times 10^9 \text{ sec}^{-2}$ and $B = 4.61 \times 10^9 \text{ sec}^{-2}$. From Eqn. 4.7, at a frequency of 21.34 MHz, one expects a minimum of 20.27 ms corresponding to the TMA tumbling motion, at $\omega\tau_{c1} = 0.616$ and another minimum of 11.74 ms corresponding to the CH_3 group reorientation at $\omega\tau_c = 0.616$. However, present investigation reveals only one broad asymmetric minimum. The Albert et al model (expressed by equation 4.15 and used for the analysis of TMA- Selenate in the previous section) fits well to the present ^1H NMR T_1 data for TMA- Phosphate, at all frequencies studied and the fit curves are shown in Fig. 4.9. The fit parameters (activation energies and pre-exponential factors) obtained for all frequencies are within the error limits (shown in the parentheses) and are given in Table 4.6.

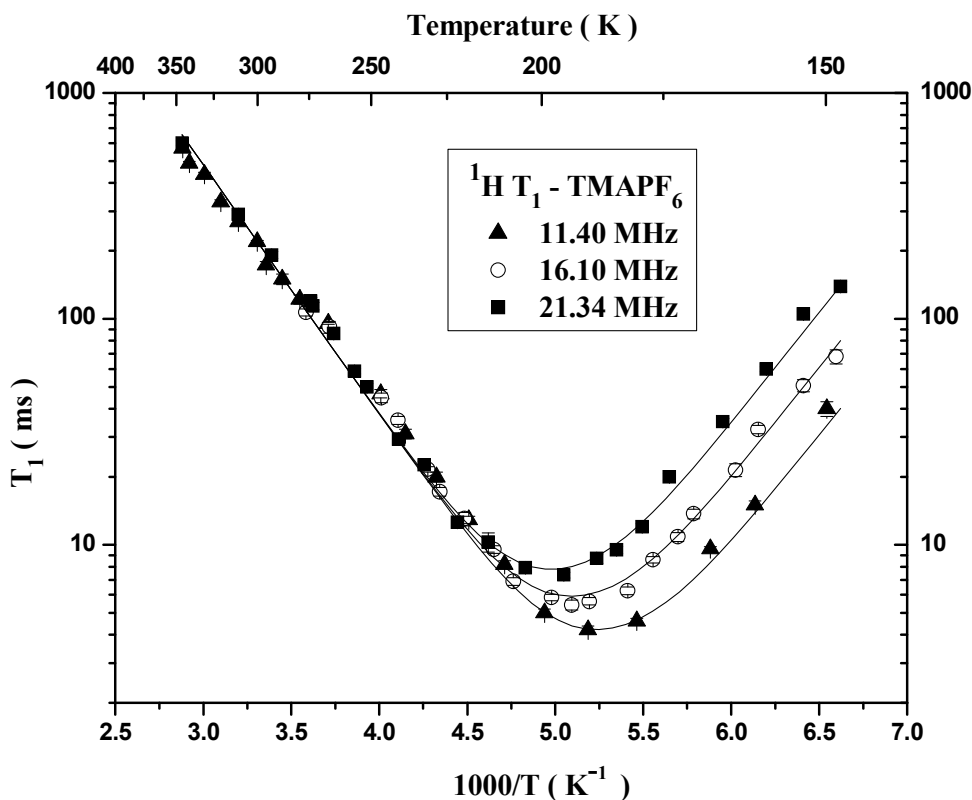


Figure 4.9 ^1H NMR T_1 data of TMA-Phosphate at 11.40 MHz (▲), 16.10 MHz (○) and 21.34 MHz (■). Solid line represents the Albert et al model fit [5].

The observed activation energies for both CH_3 and $(\text{CH}_3)_4$ ion in the present compound are lower than that observed in TMA- Selenate and hence single minimum occurs at much lower temperature than that observed in the later compound. The activation energy obtained from T_1 results (22 kJ/mol) is in excellent agreement with that (less than 24 kJ/mol) obtained from second moment studies. Also, these values are less than that of $((\text{CH}_3)_4\text{N})_2\text{SO}_4$ (28 and 45 kJ/mol), TMAClO_4 (21.2 and 32.9 kJ/mol) [23] and $(\text{CH}_3)_4\text{NX}$ (X = Cl, Br and I) (23-28 and 37-54 kJ/mol) [8]. However, they are in good agreement with those reported for other TMA compounds [64]. The CH_3 group activation energy compare well with reported value of 15-17 kJ/mol and the $(\text{CH}_3)_4$ group activation energy is slightly lesser than the reported value of 30-37 kJ/mol, for the room temperature phase of $[(\text{CH}_3)_4\text{N}]_2 \text{MX}_4$ (M=Pb and Pt ; X = Cl and Br) [24]. This indicates an increased volume for reorientation of the groups as compared to pure salts. This could be correlated to the increased volume (higher metal ion radius) available for the motion of the symmetric groups.

(b) ^{19}F NMR T_1 analysis

Figure 4.10 shows the ^{19}F NMR spin lattice relaxation time data at two larmor frequencies (16.1 and 21.34 MHz). Initially T_1 decreases with decrease in temperature from 350 K giving rise to a prominent single broad asymmetric minimum at much lower temperatures (around 100 K). On further decrease in temperature, T_1 increases with a decrease in signal intensity, at both the frequencies studied. Hence we could make measurements only up to 85 K and the signal to noise ratio decreases drastically below 85 K and the signal vanishes completely below 80 K. No measurements were possible down to liquid helium temperatures.

Theory

The analysis of the fluorine relaxation time T_1 is rather complicated compared to that of proton T_1 . Several MPF_6 compounds have been investigated by Gutowsky et al [42] by ^{19}F NMR second moment and relaxation time studies. Albert et al [46] have observed the cross relaxation effects between proton and fluorine by ^1H and ^{19}F NMR relaxation time studies in NH_4PF_6 . ^{19}F spin lattice relaxation may occur due to several reasons. Four main contributions to ^{19}F relaxation are : (a) the intra-ionic F-F interaction. (b) intra ionic F-H

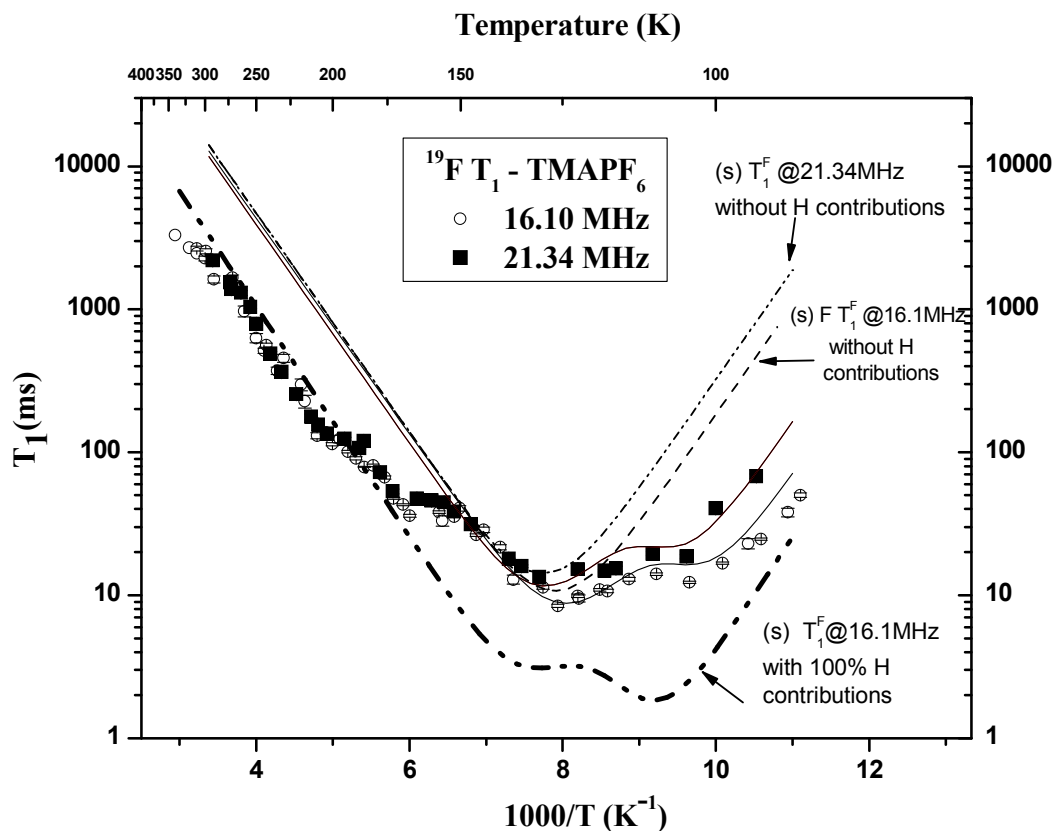


Figure 4.10 ^{19}F NMR T_1 data of TMA-Phosphate at 16.10 MHz (\circ) and 21.34 MHz (\blacksquare). Dotted lines show the simulations (s) considering only the PF_6 reorientation without considering the cross relaxation from proton. Solid lines represent the fit to Albert et al model with cross relaxation fit [46].

interaction. (c) P-F interactions and (d) interionic F-F interactions. The P-F contribution is only about 3% of the total and is neglected. Further, since the larmor frequencies of P and F differ by a factor of ≈ 0.432 , P-F cross relaxation will not play a significant role in

relaxation process. However, the cross relaxation between F and H cannot be neglected. In fact it is a prominent source for relaxation at least at higher temperatures, because the larmor frequencies of F and H differ only by a factor of 1.063. Thus ^{19}F spin lattice relaxation occurs due to the magnetic dipole – dipole interactions modulated by both the random reorientations of the PF_6 ions and random reorientation of the overall cation or methyl group.

In the high temperature region ($T > 155 \text{ K}$), the fluorine relaxation is too fast to affect spin-lattice relaxation, and hence the minima observed in the $^1\text{H } T_1$ and $^{19}\text{F } T_1$ values are due to the reorientation of protons. In accordance with the second moment data, the high-temperature proton T_1 minimum is assigned as due to the simultaneous motions of both overall rotation of the TMA ion about the N-P bond axis and reorientation of the methyl groups about C_3 axis. The relaxation rate for the fluorine nucleus can then be written as [61, 65-67]

$$\frac{1}{T_1^F} = R_F = \frac{2}{3} \gamma_F^2 \Delta M_{FF} g(\omega_F, \tau_F) + \frac{1}{2} \gamma_F^2 \Delta M_{FP} g_F(\omega_{PF}, \tau_F) + \frac{5}{48} \gamma_F^2 \Delta M_{FH} g_F(\omega_{HF}, \tau_F) + \frac{3}{16} \gamma_F^2 \Delta M'_{FH} g_F(\omega_{HF}, \tau_F), \quad (4.14)$$

where

$$g(\omega_F, \tau_F) = \frac{\tau_F}{1 + \omega_F^2 \tau_F^2} + \frac{4\tau_F}{1 + 4\omega_F^2 \tau_F^2} \quad (4.15)$$

$$g_F(\omega_{PF}, \tau_F) = \frac{\tau_F}{1 + (\omega_P - \omega_F)^2 \tau_F^2} + \frac{3\tau_F}{1 + \omega_F^2 \tau_F^2} + \frac{6\tau_F}{1 + (\omega_P + \omega_F)^2 \tau_F^2} \quad (4.16)$$

and

$$g_F(\omega_{HF}, \tau_F) = \frac{\tau_F}{1 + (\omega_H - \omega_F)^2 \tau_F^2} + \frac{3\tau_F}{1 + \omega_F^2 \tau_F^2} + \frac{6\tau_F}{1 + (\omega_H + \omega_F)^2 \tau_F^2}. \quad (4.17)$$

In the above equations, $\gamma_F = 2.5166 \times 10^4 \text{ G}^{-1} \text{ s}^{-1}$ is the gyromagnetic ratio of the fluorine nucleus; τ_F is the correlation time describing the orientations of the PF_6 ions; ω_F , ω_H and ω_P are larmor frequencies. For $\omega_F = 21.34 \text{ MHz}$, the corresponding ω_H is 22.68 MHz and ω_P is 9.18 MHz.

The quantities ΔM_{FF} and ΔM_{FP} in Eqn. 4.14 are the changes in the apparent second moment of the fluorine resonance, in G^2 , associated with the random reorientations of the PF_6 ions. The intraionic contributions to ΔM_{FF} and ΔM_{FP} depend upon the P-F bond distance in the octahedral ion. If one takes this value as 1.58\AA [50], these two contributions are found to be 12 and $1.7 G^2$, respectively [42]. ΔM_{FH} and $\Delta M'_{FH}$ represent the reduction in second moment for the H-F interactions for spherically averaged TMA ion and stationary PF_6 ions respectively. The ΔM_{FH} and $\Delta M'_{FH}$ values are assumed to be respectively, 3.1 and $3.8 G^2$ for tetrahedral symmetry for the cation [46]. Considering these factors, one can rewrite the Eqn. 4.14 as

$$\frac{1}{T_1^F} = 5.066 \times 10^9 g(\omega_F, \tau_F) + 0.5383 \times 10^9 g_F(\omega_{PF}, \tau_F) + c_1 2.045 \times 10^9 g_F(\omega_{HF}, \tau_F) + c_2 4.5126 \times 10^9 g_F(\omega_{HF}, \tau_F) , \quad (4.18)$$

The theoretical trends of the fluorine relaxation times expected from above Eqn. 4.18. are seen to be well reproduced in the experimental data (Fig.4.10.). In particular, the minimum at $(\omega_H - \omega_F) \tau_F \approx 1$ (i.e. $\tau_F \approx 1.17 \times 10^{-7}$ s, which occurs at 108 K) and a hump at $\omega_F \tau_F \approx 1$ (i.e., $\tau_F \approx 7.46 \times 10^{-8}$ s, which occurs at 111 K) which are expected [68] from the form of Eqn. 4.17 are well reproduced in the experimental fluorine relaxation time curve. If the contribution from the proton is neglected, i.e., considering only first two terms in the Eqn. 4.14, one gets single T_1 minimum of 13.34 ms at 21.34 MHz and 10.06 ms at 16.1 MHz as shown by the dotted lines in the Fig. 4.10. Further, if one considers proton relaxation is efficient throughout the temperature region studied, then the ^{19}F NMR T_1 data should have been followed by the thick dotted line shown in the Fig. 4.10. However, experimental T_1 data follows this trend from higher temperatures to about 155 K and below this temperature, it deviates significantly. It is interesting to note that, at the same temperature i.e., 155 K the 1H NMR signal becomes very weak and then vanishes completely as observed both in second moment measurements as well as in T_1 measurements. Considering all these factors, one can conclude that both methyl and TMA groups freeze below this temperature. However, still there is a finite contribution from some protons, which are still actively relaxing fluorine nuclei. By considering this model to fit the present experimental results, it may be concluded from the observed

values of C_1 (0.089) and C_2 (0.1) that, the number of protons that contribute at most may be about 10% of the total number of protons. The best-fit parameters are given in table 4.6.

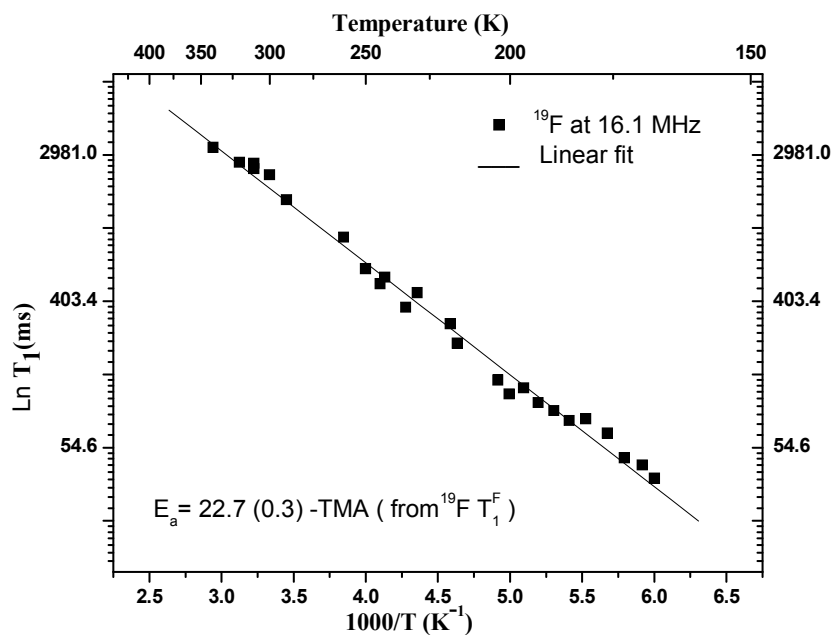
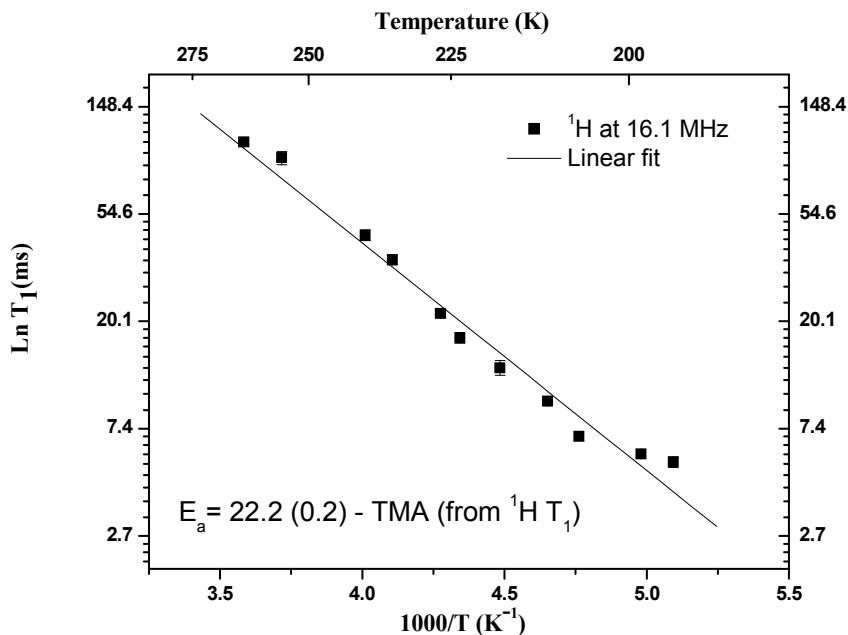


Figure 4.11 Estimation of activation energy for TMA ion in TMA- Phosphate from the linear portion of the high temperature sides of the ^1H T_1 and ^{19}F T_1 minima.

Table 4.6 Motional parameters for TMA-Phosphate obtained from ^1H T_1 and ^{19}F T_1 fit to models [5, 46].

Symmetric group	Activation energy (kJ/mol)	Pre-exponential factor (10^{-13} s)
Methyl	16.8 (0.5)	2.81 (1)
TMA	22 (1)	0.15 (0.02)
PF_6	15(1)	0.06(0.01)

Also, Eqns. 4.14 to 4.17 suggest that the linear portions of the high temperature side of the ^1H T_1 and ^{19}F T_1 minima should yield almost same activation energy. Indeed, the high-temperature linear portion of the ^{19}F T_1 data (Fig. 4.11.), gives an activation energy of 22.6 (0.5) kJ/mole, in excellent agreement with that obtained from the high-temperature T_1^{H} data (Fig. 4.9), 22 (\pm 1) kJ/mole. Fig. 4.11 shows the linear portions of high temperature sides of T_1 from which the activation energies have been estimated. Similar behaviour is observed in $(\text{CH}_3)_3\text{NPF}_5$ by McDowell et al [67]. However, ^1H NMR T_1 data appear not to get affected by the fluorine nuclei.

Reynhardt et al [51] have explained ^{31}P NMR T_1 results of TMA-Phosphate as due to the PF_6 reorientations and hence reported the motional parameters of the PF_6 ions. Present experimental results yield motional parameters, which are in excellent agreement

with the reported values. However, the existence of two phases, one with imperfections and another without imperfections as reported by Reynhardt [51] seems not to change the surrounding of at least the cation.

4.2.4 Conclusions

^1H T_1 measurements at all frequencies have shown single asymmetric minimum and is attributed to simultaneous reorientations of both CH_3 and $(\text{CH}_3)_4\text{N}$ groups. Second moment measurements made at 7 MHz also supports this. Cross correlation between proton and fluorine has been invoked to account for the observed ^{19}F T_1 data.

References

1. Latanowicz L, Medycki W and Jakubas R. *J. Phys. Chem. A*, **109(14)**, 3097 (2005).
2. Latanowicz L. *J. Phys. Chem. A*, **108(51)**, 11172 (2004).
3. Woessner DE and Snowden BS. *J. Chem. Phys.*, **47**, 2367 (1967).
4. Andrew and Canepa PC. *J. Magn. Reson.*, **7**, 429 (1972).
5. Albert S, Gutowsky HS and Ripmeester JA. *J. Chem. Phys.*, **56(7)**, 3672 (1972).
6. Albert S and Ripmeester JA. *J. Chem. Phys.*, **58(2)**, 541 (1973).
7. Tsuneyoshi T, Nakumara N and Chihara H. *J. Magn. Reson.*, **27**, 191 (1977).
8. Furukawa Y, Kiriyama H and Ikeda R. *Bull. Chem. Soc. Jpn.*, **54**, 103 (1981).
9. Prabhumirashi LS, Ikeda R and Nakamura D. *Ber. Bunsenges. Phys. Chem.*, **85**, 1142 (1981).
10. Rao CNR and Rao KJ. *Phase Transitions in Solids*. McGraw-Hill, Newyork, 1978.
11. Serr BR, Heckert G, Rotter HW, Thiele G and Ebling D. *J. Mol. Struct.*, **348**, 95 (1995).
12. Michael Malchus and Martin Jansen. *Z. Naturforsch.* **53b**, 704 (1998).
13. Iizumi M, Axe JD, Shirane G and Shimaoka K. *Phys. Rev. B.*, **15(9)**, 4392 (1979).
14. Blinc R, Južnič S, Rutar V, Seliger J and Žumer S. *Phys. Rev. Lett.*, **44**, 609 (1980).
15. Arend H, Muralt P, Plesko S and Altermatt D. *Ferroelectrics*, **24**, 297 (1980).
16. Shozo Sawada, Yoshihiro Shiroishi, Akitoshi Yamamoto, Masaaki Takashige and Mutsumi Matsuo. *J. Phys. Soc. Jpn.*, **43(6)**, 2101 (1977).
17. Shozo Sawada, Yoshihiro Shiroishi, Akitoshi Yamamoto, Masaaki Takashige and Mutsumi Matsuo. *J. Phys. Soc. Jpn.*, **44(2)**, 687 (1978).
18. Keizo Horiuchi, Shinsaku Uezato, Yumiko Yogi, Akihiko Abe, Takanori Fukami, Ryo Takeishi and Ryuichi Ideda. *Phys. Rev.*, **B72**, 174114 (2005).
19. Sato S, Endo M, Hara N, Nakamura D and Ikeda R, *J. Mol. Struct.*, **345**, 197 (1995).
20. Bloembergen N, Purcell EM and Pound RV. *Phys. Rev.*, **73 (7)**, 679 (1948).
21. Woessner DE. *J. Chem. Phys.*, **36**, 1291 (1962).

22. O'reilly DE and Tsang T. *J. Chem. Phys.*, **46**, 1 (1967).
23. Tsuneyoshi T, Nakamura N and Chihara H. *J. Magn. Reson.* **27**, 191 (1977).
24. Sato S, Ikeda R and Nakamura D. *Ber. Bunsenges. Phys. Chem.* **91**, 122 (1987).
25. Yano H, Furukawa Y, Kuranaga Y and Okuda T. *J. Mol. Struct.*, **520**, 173 (2000).
26. Senthil Kumaran S, Ramesh KP and Ramakrishna J. *Mol. Phys.* **99(16)**, 1373 (2001).
27. Sarma BS and Ramakrishna J. *Curr. Sci.*, **53**, 459 (1984).
28. Latonowicz L. *J. Concept. Magn. Reson. A.* **27(1)**, 38 (2005).
29. Horsewill AJ. *Progr. in Nucl. Magn. Reson. Spectroscopy*, **35**, 359 (1999).
30. Svare I, Raaen AM and Finland WO. *Physica B.* **128**, 144 (1985).
31. Svare I, Raaen AM and Thorkildsen G. *J. Phy. C: Solid State Phys.*, **11**, 4069 (1978).
32. Ylinel EE, Tuohi JE and Niemela LKE. *Chem. Phys. Lett.* **24**, 447 (1974).
33. Clough S, Horsewill AJ, Johnson, MR, Sutchliffe JH, Tomsah IBI. *Mol. Phys.*, **81**, 975 (1994).
34. Srenivasan R. *MTP International Review of Science, Magnetic Resonance, Series II* (ed. McDowell, C.A.) London, P209 (1975).
35. Clough S, Horsewill AJ, Johnson MR, Sutchliffe JH and Tomsah IBI. *Mol. Phys.*, **81**, 975 (1994).
36. Ingman LP, Punkkinen M, Vuorimaki AH and Ylinen EE. *J. Phy. C: Solid State Phys.*, **18**, 5033 (1985).
37. Tuohi JE and Ylinen EE, *Phys. Scr.*, **13**, 253 (1976).
38. Ingman LP, Punkkinen M, Ylinen EE and Dimitropoulos C. *Chem. Phys. Lett.* **125**, 170 (1986).
39. Koksai F, Rossler E and Sillescu H. *J. Phys. C.* **15**, 5821 (1982).
40. Müller-Warmuth W, Schüler R, Prager M and Kollmar A. *J. Chem. Phys.*, **69(6)**, 2382 (1978).
41. Miller GR and Gutowsky HS. *J. Chem. Phys.*, **39(8)**, 1983 (1963).
42. Gutowsky HS and Albert S. *J. Chem. Phys.*, **58(12)**, 5446 (1973).
43. Hiroshi Ono, Shin'ichi Ishimaru, Ryuichi Ikeda and Hiroyuki Ishida. *Bull. Chem. Soc. Jpn.*, **72**, 2049 (1999).

44. Hiroshi Ono, Shin'ichi Ishimaru, Ryuichi Ikeda and Hiroyuki Ishida. Ber. Bunsenges. *Phys. Chem.*, **102**, 650 (1998).
45. Grotte M, Kozak A, Kozil AE and Pajak Z. *J. Phys: Condens. Matter.*, **1**, 7069 (1989).
46. Albert S and Gutowsky HS. *J. Chem. Phys.*, **59(7)**, 3585 (1973).
47. Heyns AM and de Beer WHJ. *Spectrochimica Acta*, **39A(7)**, 601 (1983).
48. Staveley LAK, Grey NR and Layzell MJ. *Z. Naturforsch. A* **18**, 148 (1963).
49. De Beer WHJ and Heyns AM. *Spectrochimica Acta*, **37A**, 1099 (1981).
- 49A. United States Patents **6773822**, **20040110868**:
OSTI ID: **4572627**, **AD0757883**:
Ugalde L, Bernede JC, Del Valle MA, Díaz RF and LeRay P. *J. Appl. Polymer Science*, **84(10)**, 1799 (2002):
Al-Nakib Chowdhury, Yoshihito Kunugi, Yutaka Harima and Kazuo Yamashita. *Thin Solid Films*, **271**, 1 (1995).
50. Wang Y and Calver LD and Brownstein SK. *Acta Cryst.*, **B36**, 1523 (1980).
51. Reynhardt EC, Jurga S and Jurga K. *Chem. Phys. Lett.*, **194**, 410 (1992).
52. Mallikarjunaiah KJ and Damle R. *Vignana Bharathi*. **11(1)**, 50 (2005).
53. Van Vleck JH. *Phys. Rev.*, **74**, 1168 (1948).
54. Goc R. *J. Magn. Reson.*, **78**, 132 (1998).
55. Goc R. *Comp. Phys. Comm.*, **162**, 102 (2004).
56. Goc R. *Z. Naturforsch.* **58a**, 537 (2003).
57. Blears DJ, Danyluk SS and Bock E. *Journal of Physical Chemistry*. **72(6)**, 2269 (1968).
58. Waugh JS and Fedin EI. *Soviet Physics Solid State*, **4**, 1633 (1963).
59. Tung Tsang and Utton DB. *J. Chem. Phys.*, **64(9)**, 3780 (1976).
60. Andrew ER and Canepa PC. *J. Magn. Reson.*, **7**, 429 (1972).
61. Abragam A. *The Principles of Nuclear Magnetism*. Oxford University Press; New York, 1961.
62. Mahajan M and Nageswara Rao BD. *J. Phy. C: Solid State Phys.*, **7**, 995 (1974).
63. Sato S, Ikeda R and Nakamura D. *Ber. Bunsenges. Phys. Chem.*, **91**, 122 (1987).
64. Senthil Kumaran S, Ramesh KP, Ramakrishna J. *Mol. Phys.*, 2001; **99(16)**: 1373.

65. O'Reilly DE, Peterson EM and Tsang T. *Phys. Rev.*, **160**, 333 (1967)
66. Schurr Lert R. *Advan. Fluorine Chem.*, 5,3 1 (1965).
67. McDowell CA, Raghunathan P and Williams DS. *J. Magn. Reson.*, 32, 57 (1978).
68. Caron AP, Huttner DJ, Ragle JL, Sherk L and Stengle TR. *J. Chem. Phys.*, 47(8), 2577 (1967).